AGU PUBLICATIONS

JGR

Journal of Geophysical Research: Oceans

RESEARCH ARTICLE

10.1002/2014JC010404

Key Points:

- Fast-ice thickness varies with surface ocean temperature, as well as snow depth
- Thickness anomalies are linked to tidal enhancement of ocean heat flux
- Reductions up to 80 percent are undetectable by eye or infrared sensor

Correspondence to:
H. Melling,
Humfrey.Melling@dfo-mpo.gc.ca

Citation:
Melling, H., C. Haas, and E. Brossier (2015), Invisible polynyas: Modulation of fast ice thickness by ocean heat flux on the Canadian polar shelf, *J. Geophys. Res. Oceans*, *120*, 777–795, doi:10.1002/2014JC010404.

Received 25 AUG 2014
Accepted 29 DEC 2014
Accepted article online 7 JAN 2015
Published online 12 FEB 2015

Invisible polynyas: Modulation of fast ice thickness by ocean heat flux on the Canadian polar shelf

Humfrey Melling[1], Christian Haas[2], and Eric Brossier[3]

[1]Institute of Ocean Sciences, Ocean Science Division, Fisheries and Oceans Canada, Sidney, British Columbia, Canada, [2]Department of Earth and Space Science and Engineering, York University, Toronto, Ontario, Canada, [3]Association Nord-Est., Lanton, Hanvec, France

Abstract Although the Canadian polar shelf is dominated by thick fast ice in winter, areas of young ice or open water do recur annually at locations within and adjacent to the fast ice. These polynyas are detectable by eye and sustained by wind or tide-driven ice divergence and ocean heat flux. Our ice-thickness surveys by drilling and towed electromagnetic sounder reveal that visible polynyas comprise only a subset of thin-ice coverage. Additional area in the coastal zone, in shallow channels and in fjords is covered by thin ice which is too thick to be discerned by eye. Our concurrent surveys by CTD reveal correlation between thin fast ice and above-freezing seawater beneath it. We use winter time series of air and ocean temperatures and ice and snow thicknesses to calculate the ocean-to-ice heat flux as 15 and 22 W/m^2 at locations with thin ice in Penny Strait and South Cape Fjord, respectively. Near-surface seawater above freezing is not a sufficient condition for ocean heat to reach the ice; kinetic energy is needed to overcome density stratification. The ocean's isolation from wind under fast ice in winter leaves tides as the only source. Two tidal mechanisms driving ocean heat flux are discussed: diffusion via turbulence generated by shear at the under-ice and benthic boundaries, and the internal hydraulics of flow over topography. The former appears dominant in channels and the coastal zone and the latter in some silled fjords where and when the layering of seawater density permits hydraulically critical flow.

1. Introduction

The topic of this paper is variation in the thickness of level first-year ice. Such ice forms when the sea surface cools to freezing in autumn and continues to thicken until the weather warms—May in the Arctic. Much of the heat lost from the top of the ice via conduction and radiation into a cold atmosphere originates as latent heat of freezing liberated through ice accretion at the bottom. Thermal conduction is the dominant heat-transfer mechanism within the ice. Because the vertical temperature gradient decreases as the ice grows, so does the conductive flux and consequently the rate of ice growth (Stefan's law) [*Stefan*, 1891].

A complete time-dependent numerical simulation model of sea-ice growth was first developed by *Maykut and Untersteiner* [1971]. Their one-dimensional model simulated the changes in ice thickness over an annual freeze-thaw cycle in response to realistically specified fluxes: these included incoming solar radiation, incoming and out-going long-wave radiation, exchange of sensible heat within the turbulent atmospheric and oceanic boundary layers, change in sensible heat storage within the ice, and the release or uptake of latent heat during freezing or thawing. The model included a snow layer (wintertime accumulation, short-wave albedo, and penetration specified) and the effect of sea-ice brine pockets on specific heat capacity; top-surface temperature was calculated, not predicted. The important outcome of this work from our perspective was the demonstration that even a small depth of snow or a weak oceanic heat flux could have a large effect on ice-growth rate and end-of winter ice thickness.

Lindsay [1998] updated the calculations of *Maykut and Untersteiner* [1971] using 8 times daily measured atmospheric data in preference to climatology to force a simulation of the annual growth-ablation cycle of perennial ice in the central Arctic. His study shows that net radiation typically extracts 30 W m^{-2} from the snow surface during winter darkness, a rate 2–3 higher than the loss via sensible heat transfer through the atmosphere.

A negative correlation between end-of winter ice thickness and snow depth has been demonstrated by *Brown and Coté* [1992] using the multidecadal series of systematic observations at Canadian Arctic weather stations. *Flato and Brown* [1996] were able to replicate this inverse relationship via numerical simulation.

More recently *Dumas et al*. [2004] have shown that interannual variation in snow depth overwhelms variation in freezing-degree days (FDDs) in its effect on year-to-year variations in ice thickness; this is true under present climatic conditions in Arctic Canada, except where end-of winter snow cover is less than 10 cm [*Steiner et al*., 2013].

Any ice-growth climatology [e.g., *Ice Centre Canada*, 1992] based on these shallow locations near shore is not applicable to fast ice covering deeper less sheltered offshore waters where fast ice is established later in autumn, wind conditions, and snow accumulation are different, and there is a reservoir of sensible heat at depth in the ocean that may deliver heat to the ice via upwelling and penetrative convection. Given the strong influences of snow depth and oceanic heat flux on the thickness of first-year ice, a wide range of thicknesses within first-year fast ice is quite plausible despite common climatic forcing factors (air temperature, cloud, radiation). However, all first year ice thicker than about 30 cm looks much the same both to ice traveller and satellite. Existing satellite sensors can distinguish multiyear, first year, and young ice categories, but ice thickness determination from space is confounded by the unknown depth of snow at all electromagnetic frequencies.

There are locations in the polar oceans where very little ice accumulates in winter despite frigid conditions. These are polynyas—areas within surrounding thick ice in winter where the sea surface is ice-free or covered only by unstable new and young ice. There is an appreciable literature on the physics and oceanography of polynyas. Reviews of the subject have been prepared by *Smith et al*. [1990], *Barber and Massom* [2007], and *Williams et al*. [2007].

Polynyas have atypically thin ice cover either because ice does not form there (high influx of oceanic heat, or in spring, insolation) or because the ice that forms there does not stay there. There are two mechanisms that remove ice to expose the sea surface; strong wind (sometimes current) may push pre-existing thick ice away from an immobile boundary (fast ice or shoreline), or strong current (sometimes wind) may agitate rapidly forming small frazil crystals, preventing their consolidation into a stable ice sheet and enabling them to be carried away by current to calmer waters downdrift.

Annually recurrent polynyas on the Canadian polar shelf among the islands of the Canadian Arctic Archipelago (Figure 1) have been tabulated by *Stirling and Cleater* [1981] and *Barber and Massom* [2007]. The big ones (Cape Bathurst, Lancaster Sound, Lady Ann Strait, Smith Sound) exist primarily because the strongest winds in winter force pack ice away from the edge of fast ice. In deeper water, an upward flux of oceanic heat via wind-induced upwelling may augment the direct effect of wind [*Melling and Riedel*, 1996; *Melling et al*., 2001]. The small ones (Cardigan Strait, Hell Gate, Penny Strait, Queens Channel, Bellot Strait, Lambert Channel, etc.) have been shown to coincide with modeled local maxima in turbulence kinetic energy dissipation, proportional to u^3/d, where u is a representative speed of tidal flow and d is depth [*Hannah et al*., 2009]. These polynyas vary in size over the spring-neap cycle [*Topham et al*., 1983]. These findings implicate tidal current as a contributing factor in the formation of polynyas in fast ice, but do not identify the mechanism at work. Perhaps the oceanic heat flux is large enough in these areas to prevent the growth of new ice, or perhaps ice does form (as frazil) but cannot consolidate locally because of disturbance by strongly turbulent current.

The Canadian polar shelf is one of two important pathways for Arctic outflow to the Atlantic [*Melling*, 2000; *Beszczynska-Moeller* et al., 2011]. Only water originating in the upper 100–200 m of the Arctic Ocean can complete the transit because shallow sills on the Canadian shelf block passage of denser water from greater depth. The outflow is warm relative to freezing temperature although its temperature rarely exceeds 0°C. Its relative richness in dissolved nutrients reflects its origin in the Pacific-derived layer of the Arctic halocline, [*Alkire et al*., 2010]. Basins reaching 600 m depth to the west and east of the sills are flooded with Atlantic-derived as warm as 0.3°C. Ice observations suggest that sensible heat from this deep water does diffuse upward to warming the Arctic outflow and melt ice [*Melling et al*., 1984; *Melling*, 2002].

In this paper, we demonstrate the existence of "invisible polynyas" within the domain of first year fast ice over the Canadian polar shelf. We define "invisible polynyas" as areas where the thinning effects of oceanic heat flux and snow depth on sea ice are strong, but in contrast to traditional polynyas not so strong as to be readily evident to observers at the surface in winter. They may, however, be briefly distinguishable in summer via an earlier date of disintegration (e.g., in June or July instead of August).

We set the geographic context for this discussion with coincident wintertime observations of ice thickness and under-ice temperature from regional surveys. Next we compare time-series observations of ice growth

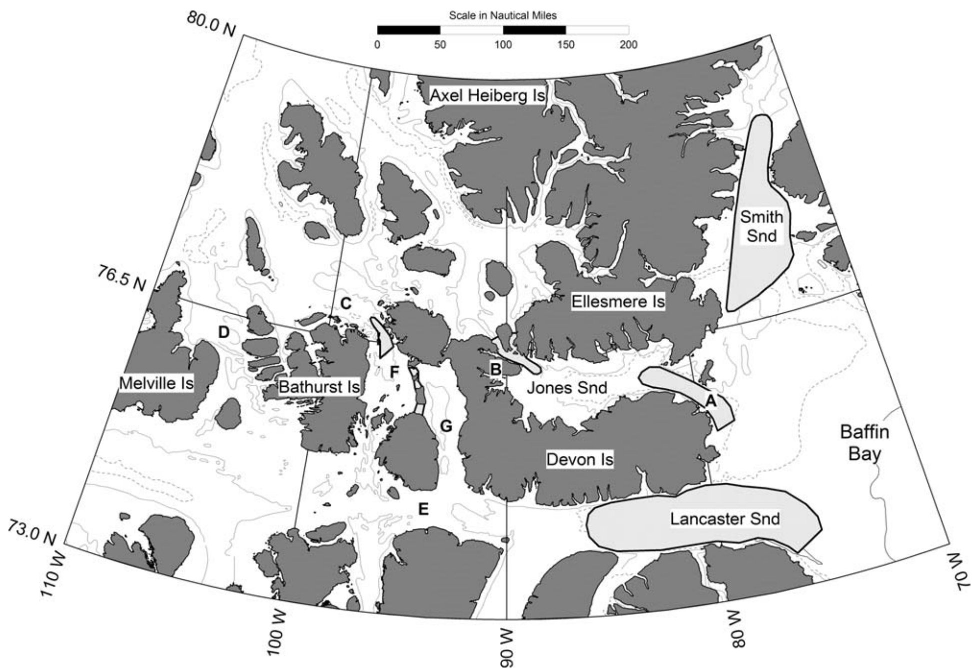

Figure 1. Area of study on the central Canadian polar shelf. Letters designate locations of interest: a: Lady Ann Strait, b: Fram Sound (with Cardigan Strait and Hell Gate), c: Penny Strait, d: Byam Martin Channel, e: Barrow Strait, f: Queens Channel, g: Wellington Channel. Light-shaded areas mark the principal polynyas in Smith Sound (North Water), Lady Ann Strait, Fram Sound, Penny Strait, Queens Channel, and Lancaster Sound. All areas to the west of the polynyas in Lady Ann Strait and Lancaster Sound are covered by fast ice in winter.

and under-ice temperature at two locations, one in Penny Strait close to small recurrent polynyas and another in Byam Martin Channel where none are known. We then move to northern Jones Sound where continuous surveys of fast-ice thickness in the winters of 2012 and 2013 lead us to the concept of "invisible polynyas." The ice thickness surveys were linked to surveys of ocean temperature and salinity, which are presented next. Finally, we present data from a freeze-to-thaw study at a reference site in South Cape Fjord (southern Ellesmere Island) where ocean temperature and salinity, snow and (unusually thin) ice were monitored at 3 day intervals throughout the winter of 2011–2012.

2. Geographic Area

The area of study is a band crossing the Canadian polar shelf at about 76°N from Byam Martin Channel in the west to Lady Ann Strait in the east (Figure 1). Since ice within this band is typically immobile (fast) between December and July, its wintertime development can be conveniently monitored.

Byam Martin Channel is dominated by cold water flowing south from the Arctic Ocean. It has a thick stable ice cover in winter and thereby is a suitable reference site against which to compare ice and ocean characteristics at locations further east—tidal polynyas in Penny and Cardigan Straits, fast ice in Jones Sound and fjords of southern Ellesmere Island, and a wind-forced polynya in Lady Ann Strait (see Figure 1 for locations).

The data central to this study were collected during the winters of 2011–2012 and 2012–2013 by one author (EB) in northern Jones Sound. During the first winter, EB was based on his yacht *Vagabond* in South Cape Fjord; the focus at this time was acquiring time series of air temperature, ice and snow thickness, and ocean temperature and salinity at a few locations in the fjord. In addition, several ice-thickness surveys were completed within and beyond the fjord. During the second winter, *Vagabond* was moved to the village of Grise Fjord; the emphasis for this winter was on wide-ranging surveys via snow-mobile of ice and seawater within Jones Sound and the fjords on its northern side; a time series was maintained near Grise Fjord but less intensively than in South Cape Fjord during the preceding winter.

Additional data have also been utilized including: regional CTD and ice thickness surveys in late winter in 1983, 1984, 1999, and 2001: T, S, and ice thickness measurements from instruments moored in Byam Martin Channel (2011–2013) and Penny Strait (2009–2010).

3. Methods

Ice thickness, freeboard, and snow depth were measured directly via drilled holes at selected sites. The accuracy of measurement was ±1 cm. Locations were accessed by snow-mobile. Several snow-only surveys were completed to document local variation in snow depth—20 measurements along a line at 5 m increments.

Wide-ranging surveys of ice-plus-snow thickness were acquired using a Geonics EM31SH electromagnetic induction (EM) sounder towed on a small sled behind a snow-mobile [e.g., *Haas et al*., 1997]. This instrument emits a 9.8 kHz EM field which propagates through the resistive sea ice and induces eddy currents in the conductive sea water. Eddy currents in turn induce a secondary EM field, whose strength is measured by the instrument. The received secondary field strength decreases with increasing distance from the conductive sea water, and thus, with increasing ice-plus-snow thickness. The EM retrievals herein are the ice-plus-snow thickness, but referred to for brevity as ice thickness. From time to time, the EM measurements were calibrated by direct measurements at colocated drill holes and comparison with theoretical EM responses, taking into account the mounting height of the EM sensor above the snow surface [*Haas et al*., 1997]. The relatively flat and uniform fast ice is an ideal target for EM ice thickness measurements because there is no ambiguity arising from the averaging of ice thicknesses within the 5–10 m wide EM footprint. The agreement between drill-hole and EM thickness measurements was ±5 cm in this study.

Ocean measurements were acquired by conductivity-temperature-depth (CTD) probe lowered to the seabed via a thin synthetic line. Because small amounts of ice in the sensing cell produce large errors in conductivity (viz., salinity) and slow down the response to change, CTD probes were kept warm between uses to avoid ice accretion on immersion. We deliberately selected CTD probes of small size that could be protected inside the operator's clothing (or in a small insulated box, thermochemically or electrically heated) and that could be passed through small diameter holes in the ice, requiring minimal drilling effort.

Three different models of CTD were used during the 2 years, with consistent calibration established through intercomparison of data. In 2011–2012, we used an Ocean Seven 304 (Idronaut S.r.l., Brugherio Italy) only 44 mm in diameter; this unit was lost when the line parted in late February. For 3 months in 2012–2013, we used an OS200 (Ocean Sensors Inc., San Diego, USA). This unit was larger (57 mm diameter) and required a more onerous 4 inch hole in the ice. A Concerto (RBR Ltd, Kanata Canada) with reduced sensitivity to ice blockage was substituted in March 2013. All models have comparable accuracy of measurement in stable conditions: ±0.002°C, ±0.005 for salinity; accuracy is further degraded when profiling.

Following the loss of the Ocean Seven CTD in 2012, the time series of temperature and salinity in South Cape Fjord was re-established on 30 April by hanging an SBE37 (Sea Bird Electronics, Bellevue, USA) from the ice at a depth of 5 m, recording data every 150 s.

4. Measurements

4.1. Regional Surveys of Ice Thickness and Under-Ice Temperature

Locally enhanced oceanic heat flux could explain the negligible ice cover of polynyas within fast ice on the Canadian polar shelf (e.g., Fram Sound, Penny Strait, Queens Channel), if it were sufficient to prevent ice growth by supplying all the sensible and radiant heat losses upward from the sea surface [*Topham et al*., 1983; *Melling et al*., 2001]. It is difficult to establish whether freezing is actually prevented in truly open polynyas because the tiny ice crystals that may form are difficult to observe and rapidly swept away by current.

Under consolidated fast ice, the process of ice formation is not ambiguous because the ice is not free to move. Local thinning of ice can only reflect local anomalies in snow depth or in oceanic heat flux; average atmospheric forcing does not vary appreciably on 100 km scale.

Ice thickness and ocean properties on the Canadian polar shelf have been surveyed during winter since the 1970s *[Birch et al*., 1983]. Data from surveys in April 1999, 2001, and 2011 are presented in Figure 2. Figure 2 top and bottom plots display the thickness of level first-year ice and the Freezing-Temperature Departure (FTD: elevation of temperature above freezing) at 5 m depth, respectively. The surveys cover all areas of interest except Jones Sound. Ice along the northern and western margins of the surveys was typically 1.8–2.1 m thick. That in the south-east was 1.0–1.8 m thick, except in eastern Wellington Channel where

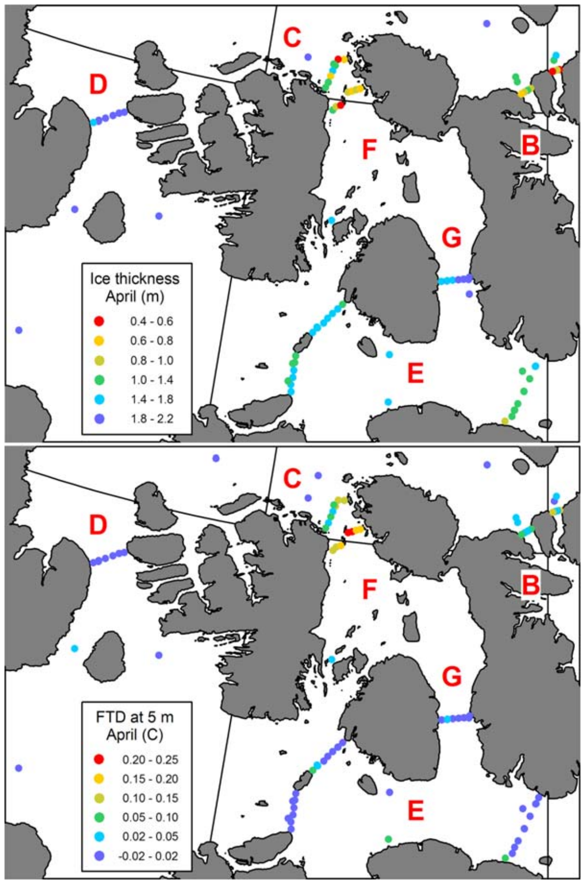

Figure 2. Thickness of level first-year fast ice measured in April via bore holes. Data from 1999, 2001, and 2011 (top). Elevation of seawater temperature above freezing at 5 m depth from depth profiles by measured CTD probe at the time of ice thickness measurement (bottom). Letters denote geographic features (see Figure 1).

thickness exceeded 1.8 m. Much thinner ice (typically 0.4–1.0 m) was measured near the polynyas in Penny Strait, Cardigan Strait, and Hell Gate. The near-surface FTD has a similar geographic pattern of variation, with values exceeding 0.2°C where ice was thinnest. The association of thin winter ice with elevated under-ice temperature (Figure 3) suggests strongly that oceanic heat flux is retarding ice growth in these areas. However, since snow depth was not measured, its possible variation across the area could plausibly be implicated.

4.2. Wintertime Growth of Fast Ice in Penny Strait

Data from an ice-profiling sonar in northwest Penny Strait during the 2009–2010 winter provide a time-series perspective on fast-ice growth. Ice draft increased from approximately 0.1 m on consolidation in early December to 1.06 m on 18 May; the latter value was confirmed by direct measurement—1.06 m draft, 1.06 m thickness, 0.19 m snow (Figure 4). The ice thickness in Resolute Bay, 250 km to the south-south-east increased from 0.65 to 1.65 m (snow depth from 0.25 to 0.50 m) over this time (data from the Canadian Ice Service). Less ice grew in Penny Strait than in Resolute Bay during this interval despite a thinner starting point and thinner snow cover. Indeed the

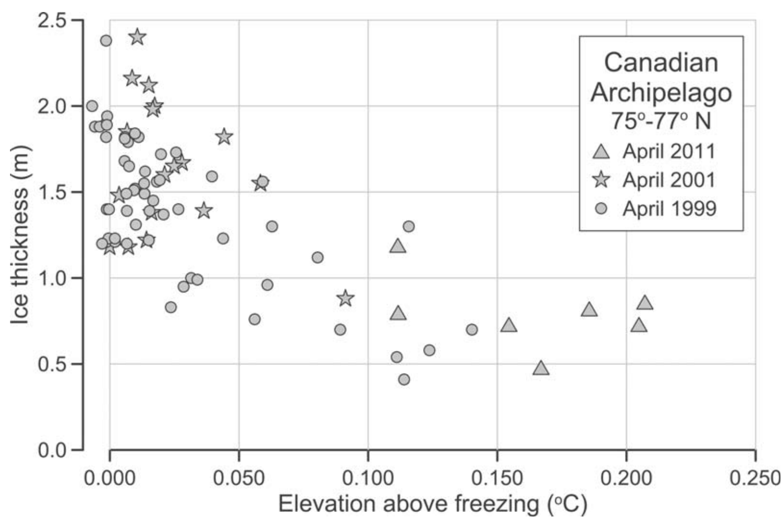

Figure 3. Scatter plot of level ice thickness against the freezing-temperature departure (FTD) of seawater at 5 m depth, from surveys in April 1999, 2001, and 2011.

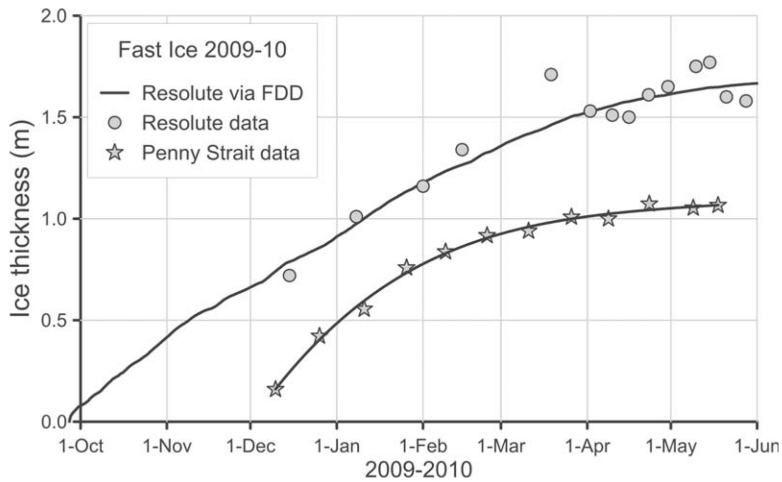

Figure 4. Comparison of fast-ice growth in Penny Strait and near shore in Resolute Bay during the winter of 2009–2010. The lower curve is a fit by least squares to the data from Penny Strait. The upper curve is a prediction for Resolute based on accumulated freezing degree-days (FDDs).

ice in Penny Strait grew less than 10 cm between mid-March and mid-May (0.16 cm/d) whereas the already thicker ice with more snow at Resolute grew 30 cm (0.5 cm/d).

4.3. Time Series of Under-Ice Temperature in Penny Strait and Byam Martin Channel

Conditions very close to the ice in Penny Strait were measured by chance for 4 days between the release of an oceanographic mooring from its anchor and its retrieval through the ice in May 2010. During this time, temperature-salinity recorders were suspended at depths of 1 and 31 m below the ice. Temperature and salinity varied appreciably on tidal and shorter time scales, by 0.25°C and 0.5 ppt at 31 m below the ice and about half these amounts at 1 m depth. The freezing-temperature departure close to the ice varied between 20 and 160 m°C (Figure 5) whereas the range at 31 m was 80–390 m°C. Clearly water warm enough to melt ice was very close to it during this entire interval in mid-May.

Although not shown here, conditions were quite different during a 5 h interval before mooring retrieval in Byam Martin Channel in April 2012: here, the temperature just below the ice was steady at 1 m°C below freezing (±1 m°C) while that at 31 m was 320 ± 5 m°C above freezing. It seems that near-surface water here was ready to freeze, a condition consistent with the 1.85 m of ice here (18 April).

4.4. Surveys of Fast-Ice Thickness in Jones Sound and Nearby Fjords in 2012 and 2013

Ice thickness surveys by EM sounder were completed via snowmobile during the winters of 2011–2012 and 2012–2013. The surveys were halted from time to time to acquire profiles of ocean temperature and salinity by CTD through drill holes and to directly measure ice thickness and snow depth to calibrate the EM sounder.

The focus of surveys during the first winter was mapping ice thickness in South Cape Fjord. Eight surveys completed between 12 February and 27 April revealed a consistent pattern of variation, with ice thicker at

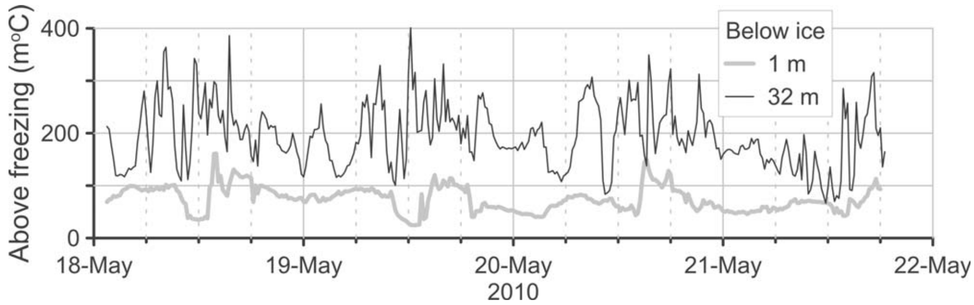

Figure 5. Freezing-temperature departure at 1 m below the ice at the location of ice-profiling sonar in Penny Strait (area C in Figure 1), May 2010 (four samples per hour).

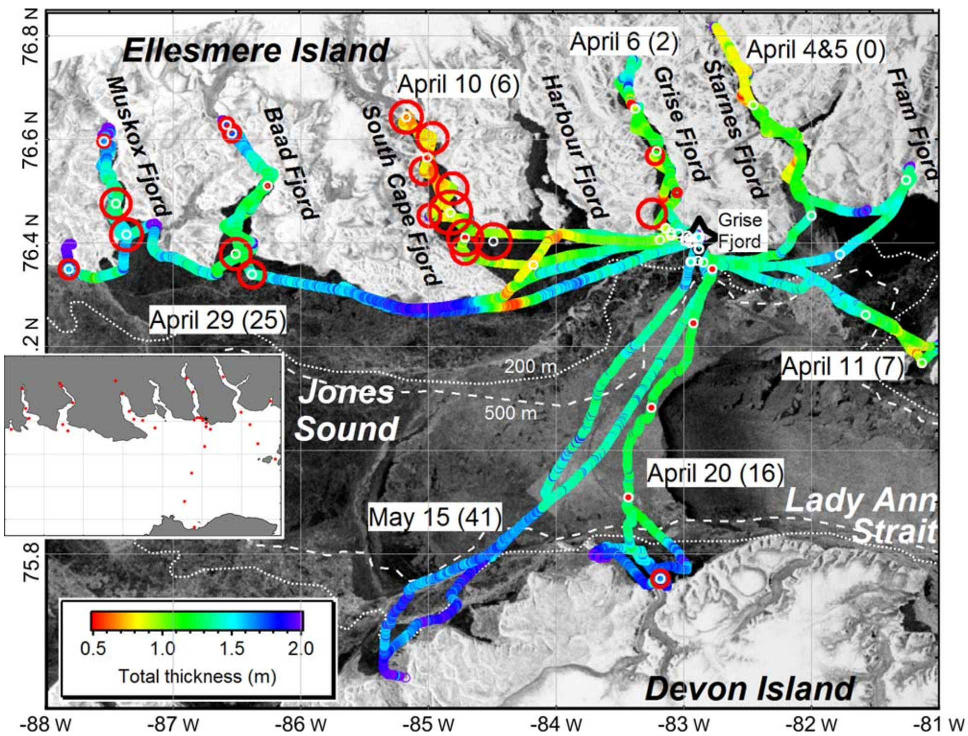

Figure 6. Jones Sound and the fjords of southern Ellesmere Island. Colored circles represent the total (ice plus snow) thickness from surveys during April–May 2013. Some fjords were visited several times, but this figure displays shows data only from the survey with widest coverage. The size of open red circles represents manually measured snow depth from 4 to 39 cm (small to large circles). The number following the indicated date of each survey is the interval in days between that date and April 4. The inset map shows locations of CTD casts. The background is a ScanSAR scene acquired by RADARSAT-2 on 4 February 2013 (Data and Products © MacDonald Dettwiler and Associates Ltd. (2013)—All Rights Reserved. RADARSAT is an official mark of the Canadian Space Agency).

the fjord's mouth than at its head, and thicker along the eastern shore than along the western. Thickness within the fjord ranged between 0.5 m at the western shore near the head to 1.5 m at the eastern shore near the mouth. Sea ice was almost 2 m thick just outside the fjord. Monthly surveys across the fjord 15 km further north revealed only a few centimeters of ice growth at the centerline after 10 March, despite 20 cm of ice growth in the shallows on the eastern side only 4 km away.

The wider ranging surveys during the second winter documented ice in Jones Sound and adjacent fjords of southern Ellesmere Island. Figure 6 displays the local geography, place names, and locations of stations visited in April and May 2013. Snow survey lines (20 points) and EM calibrations were conducted at 20 of these sites (Table 1). Snow depth was greatest in South Cape Fjord and thinnest on the late-formed ice in central Jones Sound. Within any particular fjord there was a tendency, most obvious in Grise, Baad, and Muskox Fjords, for ice to be thinner under deeper snow (Figure 7). However, there was also almost a meter of variation in ice thickness across the region even for the same depth of snow (see Figure 7). The most likely cause of this disparity is difference in oceanic heat flux because atmospheric and radiative fluxes do not vary much across a region of this size.

Figure 6 presents a color-coded representation of ice-plus-snow thickness in 2013; the size of overplotted red circles depicts the depth of snow measured independently of the EM sensor at some locations. Only data from the most comprehensive survey have been plotted where several were conducted. The view is not synoptic because the surveys spanned 41 days. Nonetheless some characteristics of regional variation are clear: ice was thicker in the western Jones Sound than in the east, and thicker on the north and south shores than in the middle; it was thinner in the upper reaches of Starnes, Grise, and South Cape Fjords but not obviously so in Baad and Muskox Fjords; ice was thin near some headlands.

Ice at the reference site near Grise Fjord grew about 9 cm while surveys were completed; snow depth decreased from 8 to 3 cm. This temporal change is convolved with geographic variations in Figure 6. To de-emphasize temporal change, the same observations have been replotted in Figure 8 as differences between

Table 1. Measurements of Ice Thickness and Snow Depth at Sites for Calibration of the EMI Sensor[a]

Latitude		Longitude		Fjord	Snow Depth (cm) Mean	Snow Depth (cm) Sigma	Date	Ice Thickness (m)
76	23.36	084	43.46	South Cape	25.0		10 Apr 2013	1.20
76	27.36	085	00.29	South Cape	20.0		10 Apr 2013	1.02
76	30.58	084	49.33	South Cape	28.0		10 Apr 2013	1.03
76	32.56	085	02.87	South Cape	24.0		10 Apr 2013	0.89
76	36.44	084	58.76	South Cape	28.0		10 Apr 2013	0.76
76	38.92	085	11.08	South Cape	29.0		10 Apr 2013	0.95
75	45.12	083	11.56	Jones	15.2	2.9	21 Apr 2013	1.64
75	54.59	083	26.56	Jones	4.8	2.8	21 Apr 2013	1.33
76	05.03	083	15.69	Jones	3.8	1.8	21 Apr 2013	1.30
76	14.82	082	55.99	Jones	4.0	1.5	21 Apr 2013	1.32
76	21.16	082	47.18	Jones	3.5	2.0	22 Apr 2013	1.44
76	37.96	086	35.45	Baad	12.2	3.5	27 Apr 2013	1.81
76	30.89	086	16.30	Baad	5.1	5.5	27 Apr 2013	1.43
76	22.90	086	31.43	Baad	28.7	6.2	27 Apr 2013	1.41
76	36.10	087	33.35	Muskox	10.1	4.9	28 Apr 2013	1.79
76	28.82	087	27.68	Muskox	27.2	9.5	28 Apr 2013	1.44
76	21.13	087	49.82	Muskox	17.1	4.2	02 May 2013	1.65
76	25.16	087	22.64	Muskox	28.8	3.4	02 May 2013	1.58
76	36.99	086	33.04	Baad	15.4	7.6	04 May 2013	1.80
76	20.56	086	23.72	Baad	24.4	10.3	06 May 2013	1.52
76	24.83	084	43.44	South Cape	31.8	2.8	11 May 2013	1.27
76	27.74	084	50.41	South Cape	39.1	3.5	14 May 2013	0.85
76	24.40	084	30.07	South Cape	32.1	4.8	14 May 2013	1.10
76	34.34	083	14.11	Grise	15.0	1.8	15 May 2013	1.08
76	30.07	083	03.64	Grise	6.3	1.1	16 May 2013	1.45
76	27.65	083	15.61	Grise	26.6	2.8	16 May 2013	0.82

[a]Those with associated sigma (standard deviation) values were derived from 100 m snow lines.

thickness at the survey site and that at the reference site on the same day. In addition to the features already noted, Figure 8 reveals reduced ice thickness near Craig Harbour and in the middle reaches of Muskox and Baad Fjords relative to Jones Sound, thicker ice at the head of Grise Fjord and very thin ice in the narrows just to the south; ice was also unusually thin in places along the western shore of Grise Fjord. Among all the fjords surveyed, ice thickness was least in South Cape Fjord. The full disparity for ice alone can be seen as yet more extreme when the 20–40 cm depth of snow here (far more than the 3–6 cm at the reference site) is subtracted.

4.5. Surveys of Ocean Temperature and Salinity Linked to Ice Surveys in 2013

Locations reached by snowmobile for ocean measurement by CTD are shown in the inset on Figure 6. Profiles were measured at two or more locations in five of the six large fjords adjoining Jones Sound. The spatial pattern of ocean properties was similar in all fjords and best illustrated by the data from South Cape Fjord (Figure 9). The plots of Figure 9 include data from wintertime reference stations on the north and south sides in Jones Sound near 83°W and also a summertime reference cast from August 2011, completed from *Vagabond*.

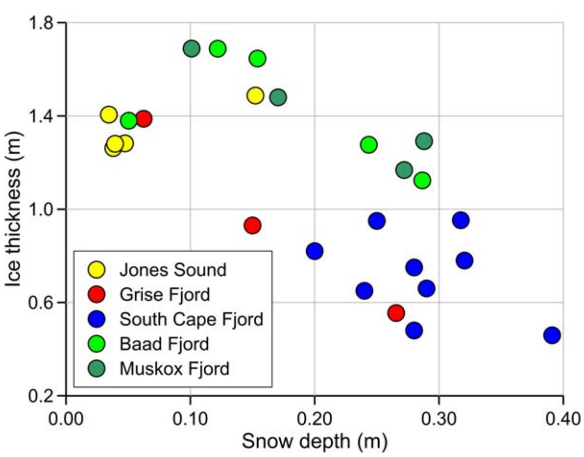

Figure 7. Ice thickness versus snow depth at 26 survey sites in late winter 2013, color-coded by location.

Figure 9 (middle plot) demonstrates that isohalines rose more than 50 m between central Jones Sound and the head of the fjord. The northward shoaling of isohalines within the Jones Sound reflects baroclinic adjustment of the Canadian Arctic through-flow—a current moving low-salinity water from the Arctic to the Atlantic [*Melling*, 2000]. A mechanism that may explain the further shoaling to the mouth

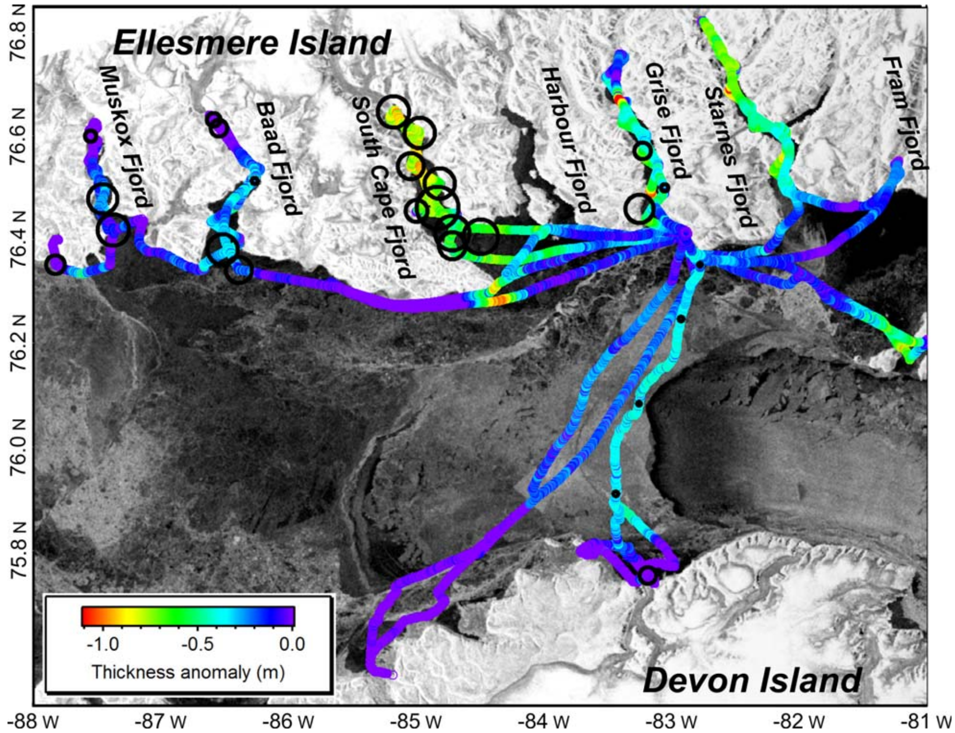

Figure 8. Geographic variation of anomalies in total (ice plus snow) thickness relative to the value on the same date at the reference site near Grise Fjord. The size of black circles represents manually measured snow depth (4–39 cm). See Figure 8 for more information. The background is a ScanSAR scene acquired by RADARSAT-2 on 4 February 2013 (Data and Products © MacDonald Dettwiler and Associates Ltd. (2013)—All Rights Reserved. RADARSAT is an official mark of the Canadian Space Agency).

of the fjord will be proposed later. Figure 9 (left) shows that water less saline than 33.2 (above 115 m depth) was much warmer in the fjord than in the sound in April 2013. Indeed the temperature-salinity curve in this salinity range was very similar to that observed out in the sound in summer (dashed curve in Figure 9). Salinity above 25 m depth in the fjord was slightly lower than any values in Jones Sound at the time.

The upward slope of isohalines placed relatively warm water, found below 50 m depth in Jones Sound, very close to the ice in the fjords. A cold surface layer here was only 5–10 m thick in April 2013, in contrast to

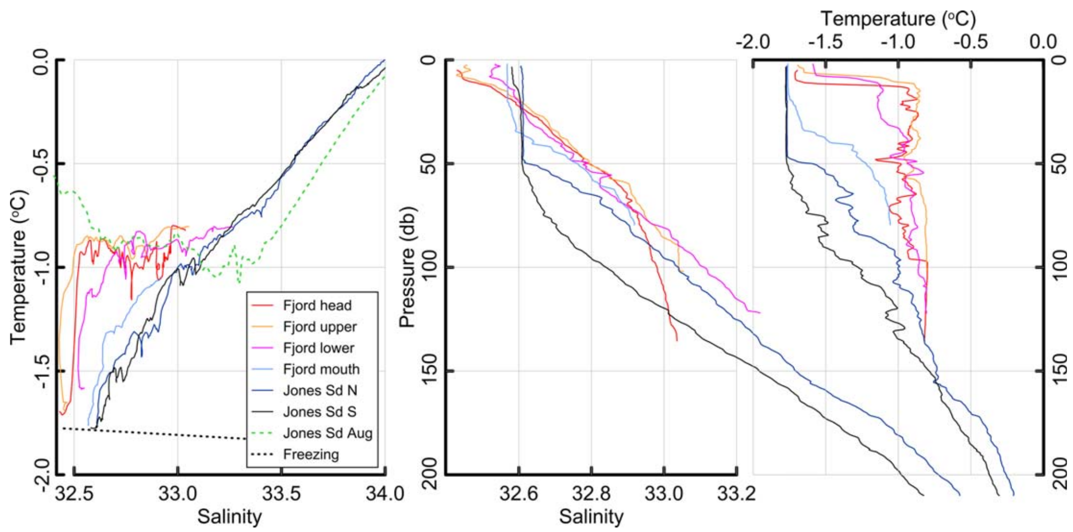

Figure 9. Temperature-salinity relationship (left) and profiles versus pressure of salinity (middle) and temperature (right) in April 2013 for a line of stations stretching southward from the head of South Cape Fjord to Jones Sound. The dashed green line on the T-S plot depicts summertime conditions in Jones Sound.

10.1002/2014JC010404

Table 2. Ocean and Sea-Ice Properties Within Fjords of Southern Ellesmere Island in April–May 2013

	Jones Sound			Fjords of Southern Ellesmere Island (Upper Reach)					
	North Side	Middle	South Side	Muskox	Baad	South Cape	Grise	Starnes	Fram
Sill depth[a], m	~	~	~	50	50	35	~	~	50
Basin depth, m	~	~	~	131	102	135	140	215	87
Effective sill depth, m	~	~	~	75	24	100	~	~	67
Date of site visit	21 Apr	21 Apr	21 Apr	30 Apr	4 May	10 Apr	6 Apr	4 Apr	4 Apr
Temperature . . . 5 m, °C	−1.77	−1.76	−1.77	−1.68	−1.65	−1.65	−1.70	−1.51	−1.69
Temperature . . 15 m, °C	−1.77	−1.76	−1.78	−1.61	−1.52	−0.85	−1.70	−1.18	−1.69
Salinity . . . 5 m	32.61	32.62	32.58	32.57	32.54	32.47	32.67	32.72	32.85
Salinity . . 15 m	32.61	32.62	32.60	32.58	32.59	32.56	32.67	32.75	32.85
FTD . . . 5 m, m°C	17	26	10	109	135	125	94	281	107
FTD . . 15 m, m°C	17	25	10	169	262	934	90	617	106
Ice thickness at site (m)	1.22	1.20	1.21	1.01	1.24	0.58	0.68	0.78	1.28
Ice thickness reference (m)	1.55	1.55	1.55	1.55	1.55	1.51	1.49	1.49	1.49
Snow depth at site (cm)	4	3	4	16	0	25	6	10	4
Snow depth reference (cm)	8	8	8	0	4	1	8	8	8

[a]Estimated from Chart No. 7310 (CHS).

50 m in Jones Sound. Moreover, water within the surface layer at 5 m depth was 100–200 m°C above freezing in the upper half of the fjords whereas in Jones Sound the FTD was only 10–25 m°C. The FTD at 15 m depth was 934 m°C in South Cape Fjord, 617 m°C in Starnes Fjord, and 262 m°C in Baad Fjord (see Table 2). These occurrences of high under-ice FTDs in the fjords were associated with thinner ice—0.58, 0.78, and 1.24 m in South Cape, Starnes, and Baad Fjords, respectively, at times when thickness values at the reference site were 1.51, 1.49, and 1.55 m.

Sills are important to the circulation of water within fjords. Shallow sills inhibit the free exchange of seawater between deep interior basins and the world outside. Unfortunately none of the fjords here is well charted (see chart No. 7310, Canadian Hydrographic Service), but there are enough soundings in Muskox, Baad, South Cape, and Fram Fjords to identify shoals across their mouths. Moreover, the chart is consistent with Grise and Starnes Fjords not having sills. Chart-based estimates of limiting depths are listed in Table 2.

It is also possible to estimate an effective sill depth by comparing vertical profiles of density within and outside fjords. The effective depth is the level outside a fjord where seawater density matches that of bottom water within the fjord. Neither method is precise but Table 2 does reveal a tendency for the effective sill depth to exceed the geometric depth in those fjords with sills.

4.6. Time Series of Ice, Snow, and Ocean Properties in South Cape Fjord During Winter 2011–2012

Vagabond spent the preceding winter, 2011–2012, frozen into ice near the northern shore of South Cape Fjord. A monitoring station was established at the middle of the fjord (76°24.801′N, 084°43.435′W; 126 m depth) on 21 October 2011 when the ice was about 30 cm thick. Ice thickness and snow depth were measured here at 3 day intervals until 1 July 2012; ocean temperature and salinity profiles were measured on the same schedule until the CTD was lost on 29 February 2012. Ocean measurements were re-established on 1 May using a continuously recording package at 5 m depth and continued until 8 July. Weather data were collected at *Vagabond* throughout.

The winter's observations are summarized in Figure 10. The curve of accumulated freezing-degree days F (top frame) is close to that observed at Resolute Bay. The equation $h=0.0137 \cdot F^{0.577}$ was used to calculate the sea-ice growth curve plotted in the second frame, where measured ice thickness and snow depth are also shown; the equation was derived from long-term average ice thickness and freezing-degree day data for Cape Parry on the Canadian polar shelf. Even early in winter ice in South Cape Fjord was growing much slower (7.5 cm/mo) than the equation predicts (35 cm/mo). By March the ice was only 70 cm thick and the growth rate had slowed to 2.4 cm/mo whereas the FDD equation predicted 153 cm ice growing 10 times faster; ice thickness at *Vagabond*'s shallow near-shore anchorage (no warm water at depth) was 112 cm.

The third frame displays FTD at the 2, 5, and 15 db levels in the ocean until late February and later at the 5 db level until July. The FTD was seldom less than 100 m°C even only 0.5 m below the ice; at times it was well over half a degree. The deeper levels were often much warmer. Despite conditions at 5 m depth, slow

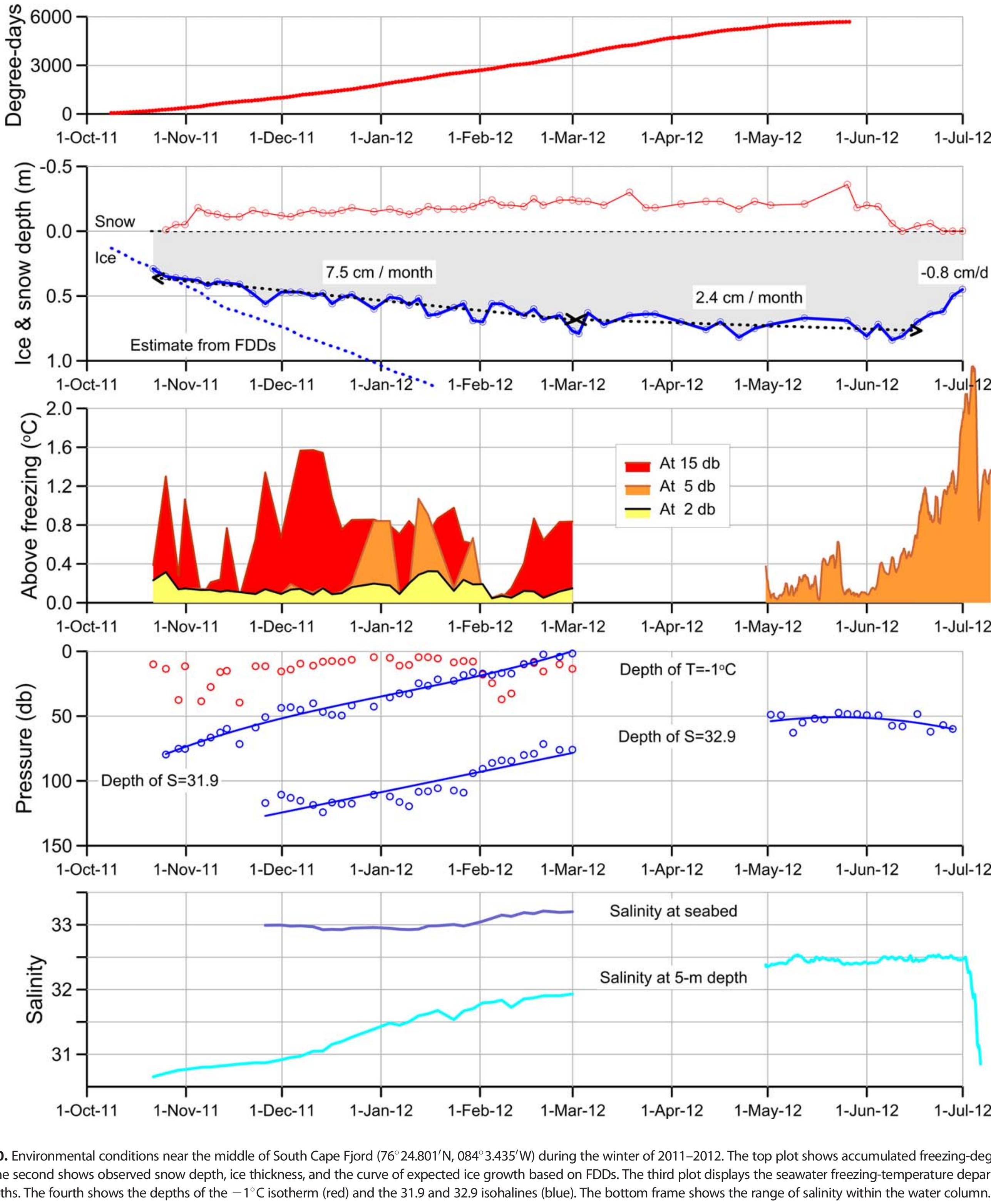

Figure 10. Environmental conditions near the middle of South Cape Fjord (76°24.801′N, 084°3.435′W) during the winter of 2011–2012. The top plot shows accumulated freezing-degree days (FDDs). The second shows observed snow depth, ice thickness, and the curve of expected ice growth based on FDDs. The third plot displays the seawater freezing-temperature departure at three depths. The fourth shows the depths of the −1°C isotherm (red) and the 31.9 and 32.9 isohalines (blue). The bottom frame shows the range of salinity within the water column.

ice growth throughout the winter indicates that an undetected thin layer of water at freezing lay just below the ice. A hint of such interfacial water was occasionally seen in CTD casts.

The next two frames display conditions deeper down: the depths of the −1°C isotherm, the depths of two isohalines, 31.9 and 32.9 and the surface and seabed salinities. The two tracked isohalines rose steadily at about

18 m/mo over the same time. The surface-salinity increase (by 1.5) reflects this prolonged upwelling while the constant depth of the -1°C isotherm indicates that heat was lost steadily from the upwelling water. Since the rising water was 1°C above freezing at depth, it carried heat toward the ice at a rate of about 30 W/m^2, a flux with the capacity to slow ice growth by 0.9 cm/d. The growth rate of ice in South Cape Fjord (0.7 m thick under 20 cm snow in early April 2012) is calculated as only 0.6 cm/d even without ocean heat flux, showing that the observed ocean heat flux was sufficient to greatly inhibit the growth of medium first-year ice there.

Salinity at the seabed in South Cape Fjord was close to 33 until late January 2012 and increased by 0.2 during February; bottom temperature was steady at $-0.75 \pm 0.01^\circ$C. However, the near-bottom 32.9 isohaline lifted during the winter at the same rate as the 31.9 isohaline, 75 m higher in the water column. These observations indicate that upwelling was driven by intrusion along the seabed at 125 m of water with 33.0–33.2 salinity. Such water was observed in northern Jones Sound at 95–125 m during the preceding summer, with temperature close to that measured in South Cape Fjord in the winter, between -1.00 and -0.85°C.

Figure 11 displays change in the near-surface temperature-salinity relationship in South Cape Fjord during the 2011–2012 winter. The curves representing conditions at 2 week intervals are coincident at the right side, showing that seawater more saline than 32.6 changed little during the winter. At lower salinity, the jagged curves are evidence of colder isohaline intrusions from elsewhere. On the left side, the endpoint of the curves shifted rightwards over time, reflecting the increase in surface salinity already noted, and near-ice temperature remained near to but not at the freezing line (dashed). The area between the curves for early winter and subsequent dates is proportional to the heat lost from the water column over the intervening time.

4.7. Thinner Winter Ice Brings Earlier Break-Up?

Views of ice in the fjords of southern Ellesmere Island are shown in Figure 12 for three dates in the summer of 2012. They reveal variations in ice color among the fjords, indicative of differences in the ice state of deterioration. Ice broke up during the 10 days followed the sequence: Starnes first, then Harbour, then South Cape, then Grise, then Muskox; Baad Fjord was still ice-covered on 10 July. The sequence is close, but not identical, to a list from thinnest to thickest ice-plus-snow based on surveys earlier in spring (Table 2): Starnes (78 + 10 cm), Harbour (unknown), South Cape (58 + 25 cm), Grise (68 + 6 cm), Muskox (101 + 16 cm), Baad (124 + 0 cm). Dates may also have been influenced by variation in ice flooding by snow-melt from land.

5. Discussion

In summary, thinner fast ice has consistently been found near polynyas in the central Canadian Archipelago than remote from them, with a correlated spatial pattern of FTD—higher with thin ice. However, since snow depth was not recorded during most surveys, attribution of thinner ice to larger oceanic heat flux is equivocal. We have measured much slower growth of fast ice near the Penny Strait polynyas than at Resolute during 2009–2010 despite thinner snow there; these observations tip the attribution in favor of oceanic heat. So also do our short records of under-ice temperature in Penny Strait and Byam Martin Channel, with the former having a 20–150 m°C FTD under 1.06 m ice and the latter -1 m°C FTD under 1.85 m ice. Our surveys of ice thickness and ocean temperature in the fjords of southern Ellesmere Island (spring 2013) have revealed under-ice FTDs of 100–200 m°C in their upper reaches and ice-thickness anomalies inversely correlated with FTD. Our overwinter monitoring study in one of the fjords (2011–2012: South Cape) has

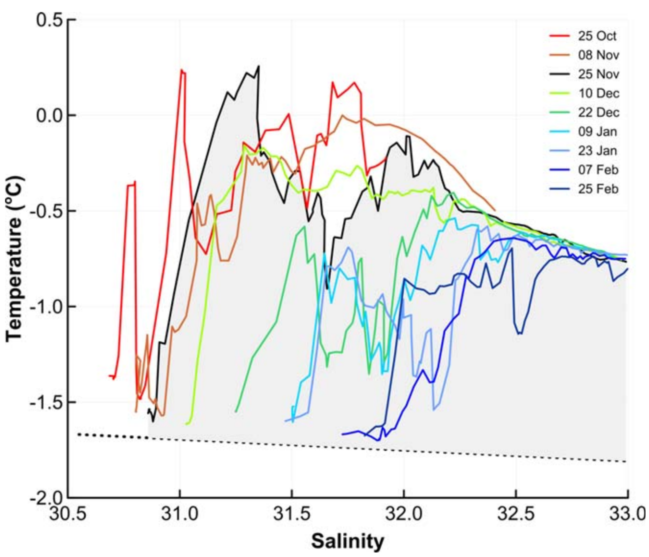

Figure 11. Change in seawater temperature-salinity relationship at the reference site in South Cape Fjord (76°24.801′N, 084°43.435′W) during the 2011–2012 winter. Salinity of 33 m was at the seabed in October and at 75 m in February (see Figure 10). The sloping-dashed line shows freezing temperature.

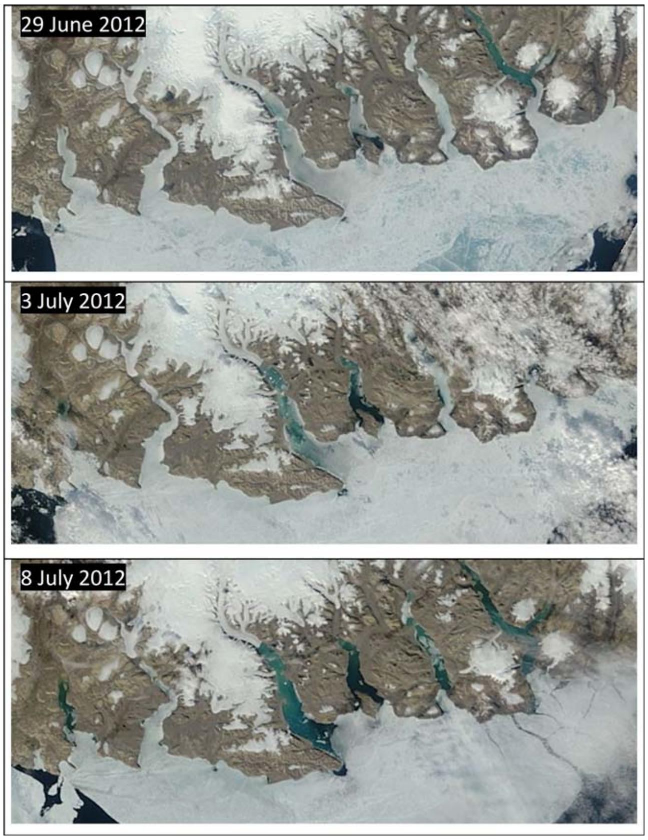

Figure 12. Satellite views of the fjords of southern Ellesmere Island in summer 2012 showing different times of ice disappearance (http://lance-modis.eosdis.nasa.gov/imagery/subsets/?project=other&subset=Ellesmere).

revealed an ice-growth rate 4–10 times slower than at Resolute Bay, consistently high under-ice FTD and steady upwelling of heat at a rate of about 30 W/m^2. Our data in combination identify oceanic heat flux as the probable culprit in the existence of "invisible polynyas."

The key issue is: How large is the oceanic heat flux? Whereas accurate time-dependent values cannot be derived from the data of this study, we can estimate the flux from ice growth rate when air temperature, snow depth and ice thickness are known [*McPhee and Untersteiner*, 1982].

A one-dimensional steady state heat conduction model with ice and snow layers suffices; the temperature of the snow surface is assumed equal to air temperature (the closest available data, from Resolute Bay, were used), that at the bottom of the ice is assumed equal to the freezing temperature and that at the ice-snow interface is calculated assuming equal fluxes within the ice and snow. The heat flux Q is:

$$Q=\alpha \cdot k_I \cdot \left(\frac{T_W-T_A}{h_I}\right) \text{ where } \alpha=\left(1+\frac{k_I}{k_S}\cdot\frac{h_S}{h_I}\right)^{-1}$$

Representative values of thermal conductivity for sea ice and wind-packed snow are $k_I = 2.03$ W/m/K [*Pringle et al.*, 2007] and $k_S = 0.31$ W/m/K [*Sturm et al.*, 2002]. The thicknesses of ice and snow are h_I and h_S, T_A and T_W are the air and water temperatures and α is the snow-layer factor—the ratio of effective conductivity to sea-ice conductivity.

The ice-growth rate is:

$$\frac{\partial h_I}{\partial t}=\left(\frac{Q-Q_W}{\rho \cdot L}\right)$$

where Q_W is the ocean heat flux, ρ is sea-ice density (920 kg m^{-3}), and L is the latent heat of fusion (3.34×10^5 J kg^{-1})

Table 3 shows the measured monthly ice thickness and estimated snow depth in Penny Strait during the 2009–2010 winter. The model permits calculation of the oceanic heat flux needed to reduce the calculated monthly average growth rate to that measured by the sonar. The result is 10–15 W/m^2. This value is close to an earlier estimate derived from the observed warming of halocline water as it moves south-eastward across the northern Canadian polar shelf [*Melling*, 2002].

The same calculation is possible with the data from South Cape Fjord, where we do have observations of snow depth in addition to ice thickness and air temperature (Figure 13). Note that the snow and ice data are "noisy" (Figure 10) because of imprecision in the measurements and local variation at the site—the drilled hole is in a different spot each time. Variation in snow depth reflects drifting and that in ice thickness reflects variation in snow depth. We use polynomial fits to smooth out the "noise" in snow and ice thickness

Table 3. Monthly Data Used To Estimate the Oceanic Heat Flux in Penny Strait During 2010[a]

	Mean Ice Thickness (m)	Estimated Snow Depth (cm)	Resolute air Temperature (°C)	Observed Growth (cm/d)	Calculated Growth (cm/d)	Ocean Heat Flux Required (W/m^2)
January	0.64	10	−30.8	0.94	1.35	14
February	0.85	15	−26.6	0.50	0.80	11
March	0.97	17	−24.8	0.29	0.69	13
April	1.03	19	−14.6	0.13	0.33	7

[a]Mean ice thickness, snow depth, and growth rate are derived from observations in Penny Strait. Air temperature at Resolute has been used to calculate ice growth rate assuming zero ocean heat flux. Ocean heat flux has been estimated from the difference between calculated and actual growth rates.

and 14 day-prior averages of air temperature because the low ice-snow diffusivity slows the freezing response to temperature change. The bottom frame shows the results: a conductive flux through the ice averaging about 30.3 W/m^2 between mid-November and April, of which about 22.6 W/m^2 (75%) over the same period originates in the ocean, not as latent heat of freezing.

The estimated values of both fluxes are lower during autumn and spring. Whereas the conductive flux will decrease with the air-sea temperature difference, air temperature is unlikely to influence oceanic flux except possibly by influencing the snow. Our assumption of seasonally invariant thermal conductivity for snow (a value typical of cold wind-packed snow) is a weakness. For the snow and ice thicknesses encountered in South Cape Fjord, the snow layer has a large effect on ice growth in winter, reducing the effective thermal conductivity α to about 33% of that of sea ice (Figure 13, top). The warmer snow of autumn and spring has higher permeability than cold snow, allowing convection to augment conductive heat transfer and increase effective the effective conductivity of the snow layer by 2–3 times [*Sturm et al*., 2002]. For the thicknesses of ice and snow measured in South Cape Fjord, this increase in snow conductivity increases heat transfer through the snow-covered sea ice by 45–70%. Our calculations assuming cold snow, therefore, underestimate both the conductive flux through the ice during autumn and spring and also the oceanic heat flux.

The sustained transfer of ocean heat to the ice in South Cape Fjord is very high by Arctic Ocean standards in winter [e.g., *Maykut and Unstersteiner*, 1971] but is only 75% of the upwelling heat flux in surface waters of South Cape Fjord discussed earlier (30 W/m^2). However, both values are miniscule compared with the flux needed to keep the sea surface free of ice in winter (500–1000 W/m^2) [*Melling et al*., 2001], as would be necessary to maintain the hypothetical yet frequently discussed "sensible heat polynya" [*Barber and Massom*, 2007].

Waters forming the halocline of Jones Sound are traceable to the Pacific Arctic inflow and, therefore, rich in dissolved nutrients [*Alkire et al*., 2010]. The observed upwelling within the fjords of southern Ellesmere Island must bring nutrients as well as warmth to the surface. Upwelled nutrients may be as important to

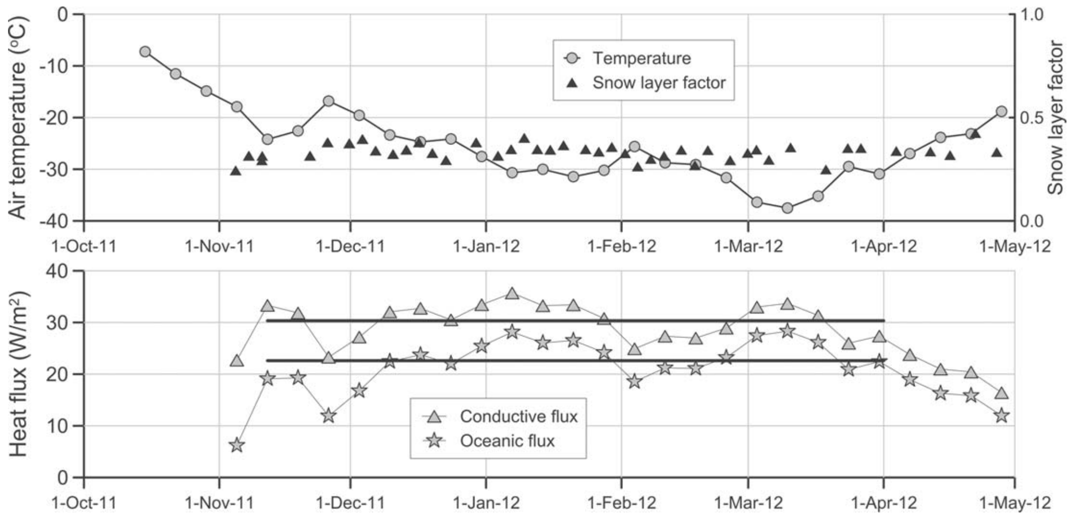

Figure 13. Weekly average air temperature in South Cape Fjord and the estimated snow-layer factor α, which is the ratio of effective conductivity to sea-ice conductivity (top). The conductive flux of heat through the ice (bottom) was calculated knowing air temperature, ice thickness, and snow depth. Also shown is the calculated flux of oceanic heat to the base of the ice that would slow ice growth to the rate observed.

local ecosystems as upwelled heat is to ice cover, perhaps explaining reports by authors EB and CH of numerous harp seal, narwhal, and seabirds in South Cape Fjord in August 2011 and by Grise Fjord residents that South Cape Fjord an excellent place to hunt ringed seal (E. Brossier, personal communication, 2011).

Traditional knowledge, our data on ice thickness and ocean characteristics and the satellite views at the time of break-up all illustrate differences among the fjords as well as similarities. Knowledge of the area is exploratory at present and does not provide a basis to explain these differences. Fjord depth and geometry, particularly the location of sills, are important missing data. The circulation pattern of water within the fjords is also unknown. Fjords at temperate latitudes generally have strong estuarine circulation driven by outflow of river-freshened water at the surface which, by entraining underlying seawater, drives an inflow at depth. Since there are no rivers flowing on Ellesmere Island in the cold of winter, there is no impetus for an estuarine circulation at this time. Wind is incapable of driving circulation in winter because the fjords are capped by fast ice.

Our data suggest that the colder intrusions appearing at salinities as high as 32.6 in South Cape Fjord do not originate within it. If they did, they would need to contact the ice somewhere at the surface so as to lose heat, but CTD casts along the axis of the fjord in the spring of 2012 provided no evidence of freezing water at the surface more saline than 32.0. A longer section the following year returned the same $\pm$0.1 uniformity of surface salinity within the fjord. The only documented reservoir of water matching the intrusions is northern Jones Sound. However, any intrusion into the depth range of the 31-9–32.9 isohalines is inconsistent with the observations of equal rates of uplift for both these isohalines. Intrusions into the top layer less saline than 31.9 are inconsistent with the need for outflow at the surface to counteract inflow at the seabed.

Outflow at the surface of South Cape Fjord is a necessary consequence of the persistent upwelling at mid-depth. If upwelling occurs at the estimated 18 m/mo throughout the fjord (6 km wide at the mouth, 2 km at the head, 24 km long), the circulation rate is 670 m^3/s. If the outflow occupies the top 10 m, its speed at the mouth would be 1 cm/s and its transit time from the head of the fjord would be about 2 months. If the inflow at the seabed occupied the bottom 5 m, its average speed would be 2 cm/s. These are weak currents.

Because energy is not available from the wind or an estuarine circulation in winter, tidal energy is the only plausible source to drive upwelling. The steadiness of upwelling in South Cape Fjord is consistent with tidal forcing, as also are the differences among the fjords of southern Ellesmere Island in the impact of upwelling on ice growth. Differences are to be expected because each fjord is topographically unique and interacts differently with the tide in dissipating energy [e.g., *Farmer and Smith*, 1980]. Although the lack of good bathymetric data precludes informed discussion of tidal influence, a continuous series of temperature-salinity data recorded in South Cape Fjord from 29 April to 10 July 2012 provides some insight.

Figure 14 shows values of temperature and salinity measured every 150 s at 5 m depth in May 2012. Both variables cycled during this 2 day interval between intervals of quiet and bursts of rapid variation. The cycle was roughly in phase with tidal elevation, with bursts occurring about half-way through the ebb and steady values re-established about half-way through the flood. Based on the late February CTD profile, the 0.4 span of salinity values during bursts implied appreciable vertical displacement, about 35 m. Figure 15 is an enlarged view of one event on 10 May, clearly showing a packet of six internal waves of about 12 min period. As appropriate, the Brunt-Vaisaila period (calculated using CTD data from February) was slightly shorter, 11 min. Water temperature was relatively low at 5 m before the event, increased by 0.2°C during the low-salinity pulses and ultimately stabilized at this higher value for about 6 h even though salinity quickly returned to its original value. This tidally mediated replenishment of warm water at the surface has obvious significance for the ice-growth rate here.

Internal waves can be generated on both flood and ebb tides by flow over a sill under the right conditions of stratification [see examples in *Farmer and Smith*, 1980]. The waves form within the pycnocline when the flow becomes critical at the sill but are initially trapped there because their phase speed is equal to but opposes the tidal current. They gain the advantage as the tide slackens, moving into the fjord after an ebb tide and away from it after a flood. The observed phase relationship between tide and near-surface wave bursts in South Cape Fjord is consistent with this known phenomenon. The evidence presented makes it likely that South Cape Fjord has characteristics favoring strong coupling between tidal flow and seabed topography near the fjord's mouth.

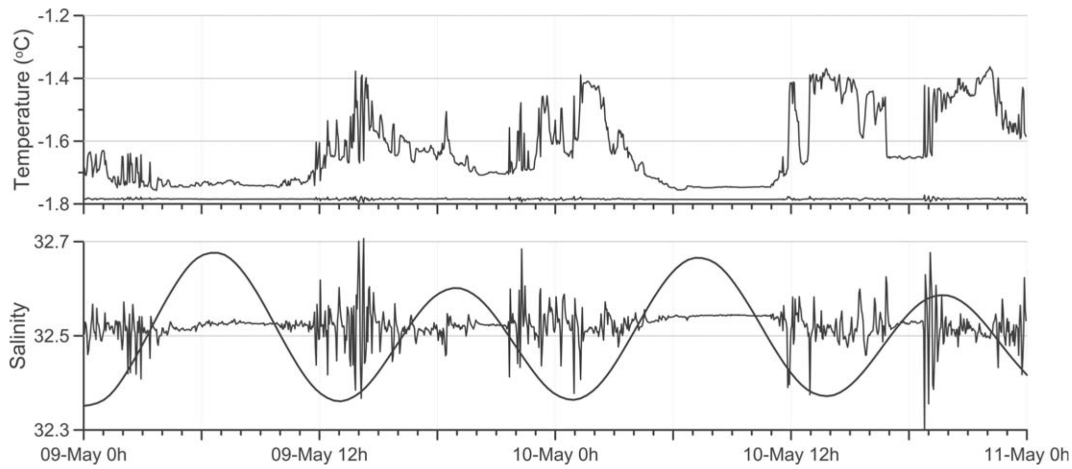

Figure 14. Variation of temperature and salinity at 5 m depth in South Cape Fjord in May 2012. The overlay on the lower frame is tidal height at the mouth of the fjord from the WebTide model [*Collins et al.*, 2011]. Data were acquired every 150 s.

Available information on the seabed topography of South Cape Fjord (Figure 16) reveals a direct route for inflow that crosses a bank of 30–40 m depth separating deeper water (120 m) to its north and south. The bank could plausibly function as a sill, since it obstructs the entrance except for a narrow circuitous pathway along the north side. The range of the semidiurnal spring tide in Jones Sound is 3.35 m [*Collins et al.*, 2011], and the corresponding spring tidal current peaks at an estimated 5 cm/s on approach to the fjord and 20 cm/s at the sill (30 m depth). CTD data were analyzed to estimate the phase speed of the first-mode internal wave; it decreased from 29 cm/s in November 2011 to 15 cm/s in March 2012. Froude number was calculated following *Farmer and Smith* [1980], using the speed of tidal flow at the sill (not that on approach because the height-above-surrounds of fjord sills typical almost blocks inflow below sill depth). The mode-1 Froude number at the sill in South Cape Fjord ranged between 0.7 (subcritical) in November and 1.3 (supercritical) in March. These estimates are consistent with tidal generation and release of lee waves at the South Cape sill, as documented elsewhere by *Farmer and Smith* [1980].

The observation of apparent tidally generated wave packets in South Cape Fjord raises the possibility that a range of hydraulic phenomena occurs here as tidal flow and stratification vary at the sill. If internal hydraulics were to enable bidirectional exchange (mode-1) at the sill, bottom water could be routinely supplied to the basin of the fjord on each ebb tide. Tidally driven bidirectional exchange over a sill has been observed in a fjord on Canada's Pacific coast by *Farmer and Denton* [1985]. During this event, on an ebb tide, low density surface water flowing outward over the sill was drawn down by a hydraulic jump on the lee side, while higher density water from mid depth on the outside flowed inward across the top of the sill and down into the fjord basin. Were the same phenomenon active in South Cape Fjord, water below sill depth within the fjord would be denser than at the same level outside and would be persistently upwelling. These characteristics have been documented in South Cape Fjord during winter (Figures 9 and 10). Moreover, the cessation of upwelling within South Cape Fjord by May (Figure 10) could reflect the change in internal hydraulic conditions with the progressive weakening of water-column stratification as low-salinity surface water was exported.

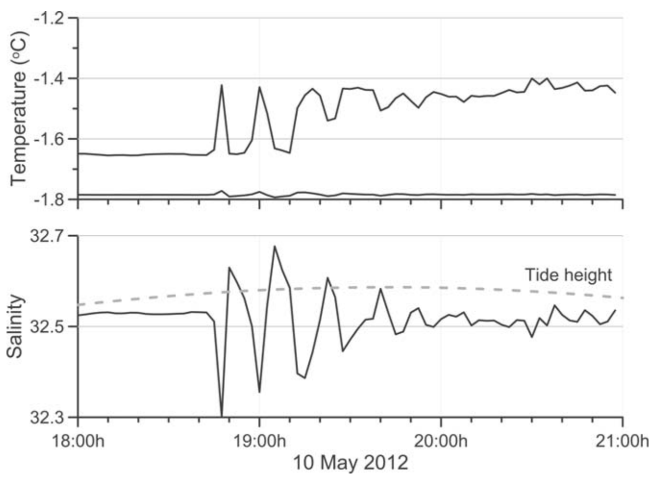

Figure 15. Three-hour data sequence at 5 m depth in South Cape Fjord showing the effect of an internal wave packet. The line at the bottom of the upper frame is freezing temperature. Data were acquired every 150 s.

10.1002/2014JC010404

6. Conclusions

The definition of a polynya—an ocean area within surrounding thick ice in winter that is ice-free or covered only by unstable new and young ice—reflects what was originally a mariner's perspective wherein the polynya's presence was readily detected by eye. This study has demonstrated that more sensitive tools of observation can find polynyas that are invisible to the human eye, ocean areas where ice cover in winter is appreciably thinner than surrounding ice. This nuance could be acknowledged in a modified definition of a polynya as an ocean area where ice cover in winter is appreciably thinner than surrounding ice and sometimes even ice-free or covered only by unstable new and young ice.

Polynyas by this expanded definition are both more extensive and more numerous over the Canadian polar shelf than previously acknowledged. Surveys of this vast area are far from comprehensive, but this study has discovered invisible polynyas in Penny Strait, MacDougall Sound, western Wellington Channel, southern Barrow Strait, within some of the fjords of northern Jones Sound and near shore above shoals and in shallow channels in many places.

The locations of invisible polynyas appear linked to the presence of seawater above freezing temperature at 5 m depth. In general, winter ice is thinner where freezing temperature departures at 5 m depth is larger. These observations are consistent with accepted flux-gradient parameterizations of boundary-layer heat transfer, wherein heat flux is proportional to temperature difference across the boundary layer.

The depth of snow has a strong influence on ice growth in winter because snow has very low thermal conductivity. Localized areas of deep snow could also create invisible polynyas, although appreciable snow-depth variation usually occurs on regional scales—too large to be judged polynyas—or on the very small scales of drifting—too small. However, as demonstrated in this study, the vagaries of mountain weather can create large differences in snow accumulation and ice thickness among nearby bays, fjords, and straits.

Tidal current is implicated in the formation of polynyas, traditional and invisible, via two mechanisms. Shear across the boundary layers of tidal flows generates turbulence that drives thermal diffusion. If the ocean is warm at depth, tidally forced diffusion enables a sensible heat flux to the ice which provides part of the heat conducted upward through the ice, resulting in less demand for latent heat and slower ice growth. Indications of a second mechanism have emerged from this study. Tidal flow into and out of fjords may interact strongly with sills at their mouths via internal hydraulic processes to generate internal (depth varying) circulation. One part may draw dense outside water over the sill and down to the bottom of the basin behind it; the inflow lifts overlying warm water within the basin inexorably toward the ice. Another part may generate energetic packets of internal waves on each ebb tide that carry kinetic energy into the fjord to drive a diffusive heat flux to the bottom of the ice.

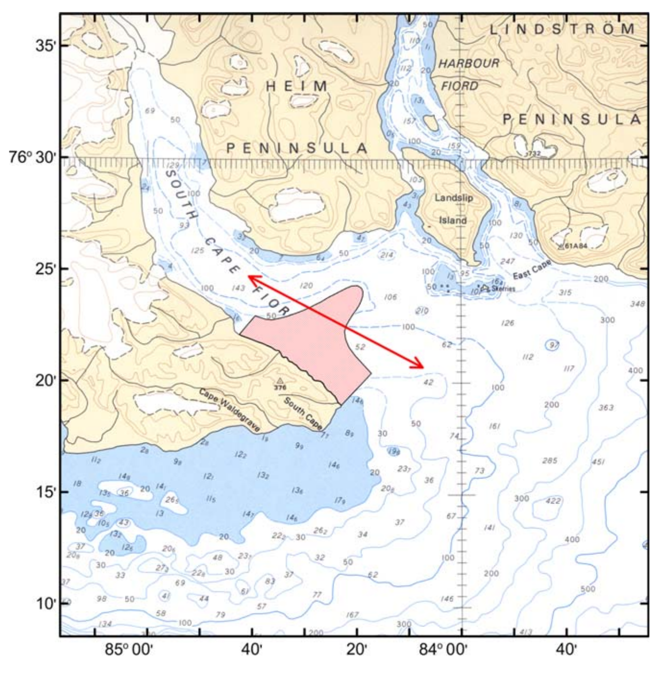

Figure 16. Seabed topography of South Cape Fjord as depicted on chart #7310 of the Canadian Hydrographic Service. Soundings are in meters. The entrance to the fjord is partly obstructed by a sill rising to less than 50 m depth (red shading) across which the tide flows (red arrow).

Observations for two consecutive winters in South Cape Fjord and in several other fjords joining Jones Sound during the second winter have demonstrated a recurrent invisible polynya in South Cape Fjord, have discovered others in the area and have shown that the tidal internal hydraulics mechanism is not equally active in all fjords there.

This study has provided estimates of ocean heat flux to the ice via both tidal-generated turbulence and tidal hydraulics mechanisms as the differences between measured and calculated rates of ice growth. The first mechanism is active in shallow straits with strong tidal current. This mechanism in Penny Strait delivers oceanic heat to the ice at a rate of about 15 W m^{-2}. The second mechanism is active in density stratified fjords with shallow sills. Active in South Cape Fjord, it moves oceanic heat upward at about 22 W m^{-2}, 2/3 of the measured upwelling flux in the ocean. In both instances, the fluxes were small enough that ice grew thick enough to make the polynya invisible but large enough that the end-of winter thicknesses were appreciably less (1.05 m in Penny Strait, 0.70 m in South Cape Fjord) than that where ocean flux was zero (1.7 m At Resolute Bay).

In both the environments studied (shallow sea strait and silled fjord), appreciable kinetic energy was available in the tide to drive upward oceanic heat flux. Nonetheless the measured values of this flux were at least 10 times too small to prevent the formation of sea ice on open water during winter in the Arctic [*Topham et al.*, 1983]. Although *Melling et al.* [2001] document times in the North Water when ocean heat flux was 300 W m^{-2}, such large values occurred only with very strong wind, ice-free seas, and very high freezing rate. Even under these conditions, the high oceanic flux provided only about 1/3 of the total loss of heat at the surface.

Invisible polynyas briefly become visible ones in early summer because their thinner ice cover breaks up earlier.

Invisible polynyas occur where there is warm water within the halocline and a mechanism (mixing or upwelling) to move it to the surface. In the Canadian Arctic, these same mechanisms bring nutrients to the surface because nutrient concentrations are high within the halocline. Invisible polynyas may, therefore, be indicators of biological hotspots.

Acknowledgments
This project was supported by the Canadian Program of Energy R&D under project B21.002, by the Alberta Ingenuity Scholarship and Canada Research Chair programmes, and by the Natural Sciences and Engineering Research Council (NSERC) of Canada. Jo Poole provided custom equipment for the oceanographic surveys by snow machine, Ron Lindsay prepared and maintained instruments and Christine Michel provided an Idronaut CTD. Mary O'Brien joined *Vagabond* to collect ocean data throughout the area in August 2011. As always, logistic support from Canada's Polar Continental Shelf Program (projects 106-12, 103-13, 633-11, 639-12) was essential to the success of this project. Ocean data from Fisheries and Oceans Canada (IOS cruise Nos. 1999-07, 2001-16, 2011-06, and 2013-21) can be searched at http://www.pac.dfo-mpo.gc.ca/science/oceans/data-donnees/search-recherche/profiles-eng.asp and are available via the data manager link or on request to Humfrey.Melling@dfo-mpo.gc.ca. Ice and snow data from the York University surveys are available on request to haasc@yorku.ca.

References

Alkire, M. B., K. K. Falkner, T. Boyd, and R. W. Macdonald (2010), Sea ice melt and meteoric water distributions in Nares Strait, Baffin Bay and the Canadian Arctic Archipelago, *J. Mar. Res.*, *68*, 767–798, doi:10.1357/002224010796673867.

Barber, D. G., and R. A. Massom (2007), The role of sea ice in Arctic and Antarctic polynyas, in *Polynyas: Windows to the World, Elsevier Oceanogr. Ser. 74*, edited by W. O. Smith and D. G. Barber, pp. 1–54, Elsevier, Amsterdam, doi:10.1016/S0422-9894(06)74002-8.

Beszczynska-Moeller, A., R. Woodgate, C. Lee, H. Melling, and M. Karcher (2011), Arctic oceanic gateways synthesis, *Oceanogr. Mag.*, *24*(3), 82–99, doi:10.5670/oceanog.2011.59.

Birch, J. R., D. B. Fissel, D. D. Lemon, A. B. Cornford, R. A. Lake, B. D. Smiley, R. W. Macdonald, and R. H. Herlinveaux (1983), Arctic data compilation and appraisal 3: Northwest passage: Physical oceanography, Canadian data report hydrography and ocean science, Inst. of Ocean Sci., Sidney BC, Canada, viii + 1262 pp.

Brown, R. D., and P. Coté (1992), Interannual variability of landfast ice thickness in the Canadian High Arctic 1950-89, *Arctic*, *45*, 273–284.

Collins, A. K., C. G. Hannah, and D. Greenberg (2011), Validation of a high resolution modelling system for tides in the Canadian Arctic Archipelago, *Can. Tech. Rep. Hydrogr. Ocean Sci., 273*, vii + 72 pp.

Dumas, J., E. C. Carmack, and H. Melling (2004), Climate-change impacts on the Beaufort shelf land-fast ice, *Cold Reg. Sci. Technol.*, *42*, 41–51.

Farmer, D. M., and R. A. Denton (1985), Hydraulic control of flow over the sill in Observatory Inlet, *J. Geophys. Res.*, *90*, 9051–9068.

Farmer, D. M., and J. D. Smith (1980), Tidal interaction of stratified flow with a sill in Knight Inlet, *Deep Sea Res., Part A*, *27A*, 239–246, doi:10.1016/0198-0149(80)90015-1.

Flato, G. M., and R. D. Brown (1996), Variability and climate sensitivity of landfast Arctic sea ice, *J. Geophys. Res.*, *101*, 25,767–25,778.

Haas, C., S. Gerland, H. Eicken, and H. Miller (1997), Comparison of sea-ice thickness measurements under summer and winter conditions in the Arctic using a small electromagnetic induction device, *Geophysics*, *62*,749–757.

Hannah, C. G., F. Dupont, and M. Dunphy (2009), Polynyas and tidal currents in the Canadian Arctic Archipelago, *Arctic*, *62*, 1–12.

Ice Centre Canada (1992), *Ice Thickness Climatology 1961–1990 Normals*, ISBN 0660573385, 277 pp., Queen's Printer, Minist. of Supply and Serv. Ottawa, Canada.

Lindsay, R. W. (1998), Temporal variability of the energy balance of thick Arctic pack ice, *J. Clim.*, *11*, 313–333.

Maykut, G. A., and N. Untersteiner (1971), Some results from a time-dependent thermodynamic model of sea ice, *J. Geophys. Res.*, *76*, 1550–1575.

McPhee, M. G., and N. Untersteiner (1982), Using sea ice to measure vertical heat flux in the ocean, *J. Geophys. Res.*, *87*, 2071–2074.

Melling, H. (2000), Exchanges of freshwater through the shallow straits of the North American Arctic, in *The Freshwater Budget of the Arctic Ocean, Proceedings of a WCRP/AOSB/NATO Advanced Research Workshop*, Tallinn, Estonia, April 1998, pp. 479–502, Kluwer Acad., Amsterdam.

Melling, H. (2002), Sea ice of the northern Canadian Arctic Archipelago, *J. Geophys. Res.*, *107*(C11), 3181, doi:10.1029/2001JC001102.

Melling, H., and D. A. Riedel (1996), Development of seasonal pack ice in the Beaufort Sea during the winter of 1991-92: A view from below, *J. Geophys. Res.*, *101*, 11,975–11,992.

Melling, H., R. A. Lake, D. R. Topham, and D. B. Fissel (1984), Oceanic thermal structure in the western Canadian Arctic, *Cont. Shelf Res.*, *3*, 233–258.

Melling, H., Y. Gratton, and G. Ingram (2001), Ocean circulation within the North Water Polynya of Baffin Bay, *Atmos. Ocean*, *39*, 301–325.

Pringle, D. J., H. Eicken, J. Trodahl, and L. G. E. Backstrom (2007), Thermal conductivity of landfast Antarctic and Arctic sea ice, *J. Geophys. Res.*, *112*, C04017, doi:10.1029/2006JC003641.

Smith, S. D., R. D. Muench, and C. H. Pease (1990), Polynyas and leads: An overview of physical processes and environment, *J. Geophys. Res.*, *95*, 9461–9479.

Stefan, J. (1891), Uber die theorie der eisbildung insbesondere uber die eisbildung im polar mere, *Ann. Physik. 3rd Ser.*, *42*, 269–286.

Steiner, N., et al. (2013), Climate change assessment in the Arctic Basin Part 1: Trends and projections: - A contribution to the Aquatic Climate Change Adaptation Services Program, *Can. Tech. Rep. Fish. Aquat. Sci., 3042*, xv + 163 pp.

Stirling, I., and H. Cleator (1981), Polynyas in the Canadian Arctic, *Can. Wildlife Serv. Occas. Pap. 45*, 70 pp., Avail. Can. Wildlife Serv., Environment Canada, Ottawa, Canada.

Sturm, M., D. K. Perovich, and J. Holmgren (2002), Thermal conductivity and heat transfer through the snow on the ice of the Beaufort Sea, *J. Geophys. Res.*, *107*(C10), 8043, doi:10.1029/2000JC000409.

Topham, D. R., R. G. Perkin, S. D. Smith, R. J. Anderson, and G. Den Hartog (1983), An investigation of a polynya in the Canadian Archipelago 1, Introduction and Oceanography, *J. Geophys Res.*, *88*, 2888–2899.

Williams, W. J., E. C. Carmack, and R. G. Ingram (2007), Physical oceanography of polynyas, in *Polynyas: Windows to the World, Elsevier Oceanogr. Ser.74*, edited by W. O. Smith and D. G. Barber, pp. 55–85, Elsevier, Amsterdam, doi:10.1016/S0422-9894(06)74002-8.